Original Research

Spatio-Temporal Bandwidth-Based Acquisition for Dynamic Contrast-Enhanced Magnetic Resonance Imaging

Sumati Krishnan, MS and Thomas L. Chenevert, PhD*

Purpose: To develop a k-space formalism that provides a rationale for the design of variable-rate acquisition schemes for dynamic contrast-enhanced magnetic resonance imaging (DCE-MRI).

Methods and Materials: The formalism, termed spatio-temporal bandwidth-based (STBB) analysis, is demonstrated using a priori modeling of object and enhancement characteristics typically observed in DCE-MRI of breast tumors. A temporally enhancing lesion is considered as a two-dimensional (2D) *space-time* object that possesses a corresponding *spatio-temporal* (k_y-k_t) energy spectrum. The k_y-k_t space is segmented based on a threshold such that the total spectral energy in a finite number of k-space samples, constrained by the imaging experiment, is maximized. This thresholded map contains a set of spatial and corresponding temporal sampling prescriptions. These prescriptions are used in designing an acquisition scheme that is adequate for a range of contrast-enhancing breast lesions. The STBB scheme is compared to an equivalent "keyhole" acquisition, in terms of quantification of enhancement rate, K^{trans}, extracellular volume fraction, v_e, and spatial fidelity. We chose object sizes Npix = 2, 5, 10, 15, 20, and 30 pixels and enhancement rates K^{trans} = 1.5, 1, 0.6, 0.4, 0.3, and 0.2 minute^{-1}, and v_e was held at 0.3.

Results: The STBB scheme results in more accurate estimation of the rate and extracellular volume fraction parameters when the object size is small (two and five pixels) and the enhancement rates are rapid (1.5 and 1 minute^{-1}), compared to the keyhole acquisition. The STBB scheme provides higher spatial fidelity for very small objects. For large object and slow enhancements, the keyhole and STBB scheme perform comparably.

Conclusion: We have demonstrated an intuitive formalism applicable to DCE-MRI for a set of targeted/anticipated dynamic events as well as spatial features. This formalism can be extended to any dynamic imaging condition, and a corresponding variable-rate acquisition scheme can be designed.

Key Words: spatio-temporal; k-space; dynamic MRI; contrast-enhanced MRI; fast imaging
J. Magn. Reson. Imaging 2004;20:129–137.

DYNAMIC MAGNETIC RESONANCE IMAGING (MRI) has been applied to several fields, including blood oxygen level-dependent (BOLD) signal response in functional MRI (fMRI) (1,2), cardiac imaging (3,4), and multiphase contrast-enhanced angiography (5–7). In particular, dynamic contrast-enhanced (DCE)-MRI to characterize tumors, e.g., in liver, prostrate, and breast, by way of contrast enhancement properties is the subject of ongoing research (8–13). For a given clinical case, the relative diagnostic importance of spatial over temporal information is not known a priori. The optimum will depend on both the spatial feature content of the lesions and the physiological information that can be elicited from the MRI data. While the clinical significance of this information is a subject of much debate, it is generally agreed that for breast tumors high-spatial-resolution imaging combined with analysis of gadolinium (Gd)-diethyltriamine pentaacetic acid (DTPA) kinetics can be used to improve specificity and sensitivity in diagnosis (14–18).

A k-space representation applicable to dynamic imaging was previously presented by Xiang and Henkelman (19). They represented the dynamic object in a k_x-k_y-t space as a combined function of the spatial frequencies and an additional temporal variable, and suggested that for dynamic imaging there existed the potential to trade off spatial and temporal samples. They, and subsequently others, have used this approach in cases where the dynamic function is quasi-periodic, such as cardiac cycles and respiratory motion or event-based fMRI (20–22). For DCE-MRI, however, it is required that a continuous aperiodic temporal function be sampled while imaging the tissues of interest. Short

Department of Radiology-MRI, University of Michigan Health System, Ann Arbor, Michigan.

Contract grant sponsor: U.S. Army Medical Research and Material Command; Contract grant number: DAMD-17-94-J-4381; Contract grant sponsor: National Cancer Institute of NIH, Public Health Services grants; Contract grant numbers: R24CA83099, P30CA46592.

This work was presented as a poster at ISMRM 2000.

*Address reprint requests to: T.L.C., 1500 E. Medical Center Dr., Department of Radiology—MRI, University of Michigan Health System, Ann Arbor, MI 48109-0030. E-mail: tlchenev@umich.edu

Received October 31, 2003; Accepted February 17, 2004.
DOI 10.1002/jmri.20090
Published online in Wiley InterScience (www.interscience.wiley.com).

TR rapid imaging methods such as spoiled gradient recalled echo (SPGR), echo-planar imaging (EPI), and spiral imaging have been employed for DCE-MRI (23–25). Ultimately, there exist scanner hardware restrictions that limit the imaging rates. This poses a trade-off between the maximum spatial and/or temporal resolution that may be achieved in DCE-MRI.

Several dynamic imaging methods that tailor coverage of the combined k_x-k_y-t space by variable-rate sampling along one or more spatial dimensions have been previously developed (25–27). In most methods it is assumed that the bulk of the dynamic change is encoded in the lower spatial frequencies. Hence, central k-space lines are sampled at a higher rate than peripheral k-space lines. This permits an increase in the overall temporal sampling rate. The extents of central k-space as well as sampling rates are somewhat arbitrarily selected. While reconstructing variably sampled data, peripheral k-space lines that are not acquired are approximated in different ways. In "keyhole" acquisition, for example, a single precontrast full-matrix acquisition is used to provide peripheral k-space data that are combined with each central k-space dynamic data set to generate a high-resolution data set (25).

A method that specifically addresses the issue of spatial-temporal resolution balance when the dynamic event is not inherently band limited is the object of this paper. As indicated earlier, the optimal balance is typically not known in clinical situations. To date, the diagnostic utility of enhancement parameters such as permeability coefficient has not been established. Regardless of the diagnostic algorithm used, however, accuracy of diagnosis is dependent on the fidelity in measuring the features of interest. The intention, therefore, is to maximize the information content of the acquired data. As a surrogate for information content, the proposed spatio-temporal bandwidth-based (STBB) formalism uses spectral energy content. The multidimensional dynamic imaging experiment is posed in terms of traversing a two-dimensional (2D) spatio-temporal (k_y -k_t) spectral map. Retrospective evaluation of full sequential vs. keyhole acquisitions in terms of errors in spectral energy coverage was recently reported (28). In this work we prospectively use the instantaneous spectral power of the modeled anticipated/targeted object as the discriminant to select appropriate temporal and spatial samples in designing the variable-rate acquisition. Prioritization of spectral samples by an energy criterion is an extension of previous concepts of preferentially acquiring only the lower spatial frequencies due to their higher energy content. Therefore, in this work we compare the performance of the STBB modeling-based acquisition scheme to that of keyhole imaging.

METHODS

STBB Analysis

The STBB method is developed by considering spatial and temporal characteristics of a targeted object, as well as specifying a set of imaging constraints. Analysis of spatial features is specific to the anatomy of interest. For example, one might target single voxels in the brain, such as in fMRI, or obtain statistics from a large diffuse area of enhancing tumor. Similarly, the temporal timescale of interest may be short (~seconds), as in an abrupt hemodynamic response, or several minutes for contrast agent equilibration. The STBB approach is illustrated using examples of morphologic features and pharmacokinetic properties of breast lesions (29). The pulse sequence used here in modeling is a three-dimensional (3D) SPGR acquisition with a TR of 10 msec that was previously used for keyhole imaging of clinical breast data at our institution (25).

Modeling of Spatial Characteristics

To simplify the STBB analysis, 3D imaging is reduced to a single spatial axis, by the following arguments. For clinical breast imaging at our institution we used a 3D sequence to permit volume coverage with significant speed advantages over an equivalent 2D sequence. Lesion analysis, however, was performed on a slice-by-slice basis in the x-y plane; hence, optimization of spatial resolution along the z-axis is not considered. Further, since the pulse repetition time, TR, is relatively short (~10 msec), frequency encoding, chosen to be along the x-axis, occurs almost instantaneously. For a conventional 3D phase encoding, it can be assumed that the faster phase encoding, say z-axis, also occurs fairly rapidly (typically < 0.5 seconds) relative to the rate of contrast uptake. The most significant contrast change can now be modeled as occurring during the slow phase-encoding dimension, i.e., the y-axis. For simplicity of analysis, lesion morphologic features are modeled in one dimension by simple rectangular functions whose width is equal to the cross-sectional diameter of the lesion.

Modeling of Temporal Characteristics

For simulations, lesion enhancement profiles are generated using a multicompartmental pharmacokinetic model developed by Tofts and Kermode (30). In this model, the lesion contrast kinetics are quantified by two standardized parameters (31): volume transfer constant K^{trans} and extracellular volume fraction ν_e. Figure 1a shows an example of an enhancement profile, *C(t)*, generated using this model with $K^{trans} = 0.4$ minute^{-1} and $\nu_e = 0.3$.

Definition of Imaging Bandwidths

The rate of imaging, which limits the achievable sampling bandwidths along the spatial and temporal axes, is a function of the pulse repetition time, TR, and the desired spatial resolution. For the simplified one-dimensional (1D) model, the rate of imaging along k_y alone is of interest. The sampling interval Δt between k-space acquisitions along k_y is the time taken to acquire one frame in the k_x-k_z plane, given as

$$\Delta t = \mathrm{TR} \times Nz \qquad (1)$$

where Nz is the matrix size along the z-encoding axis.

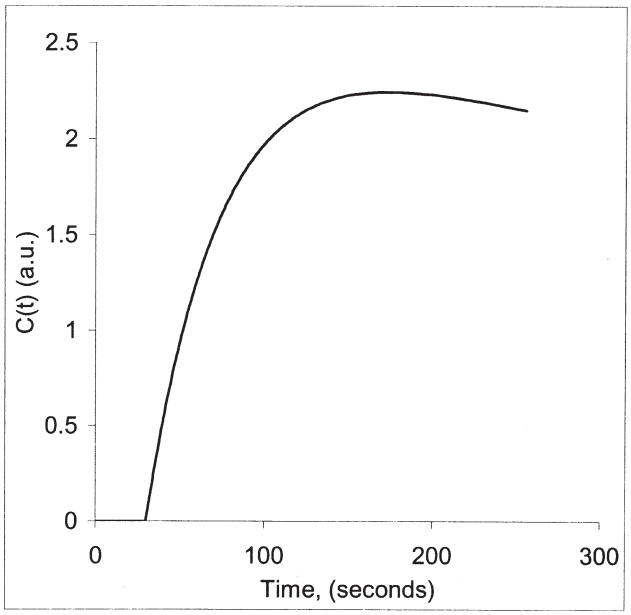

a.

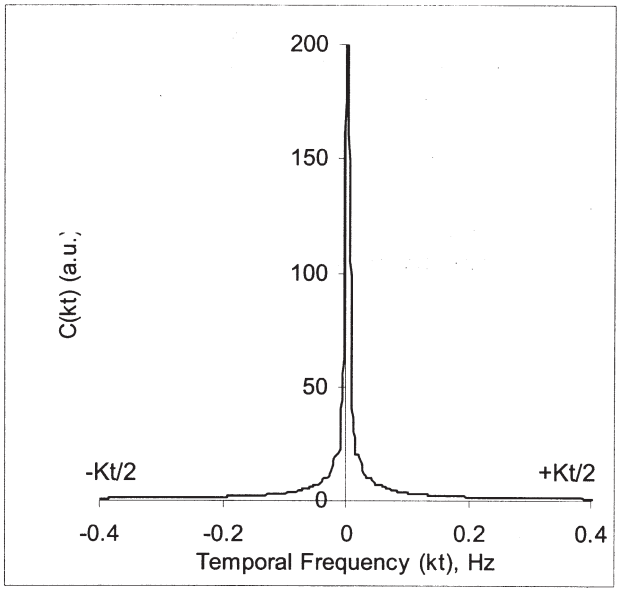

b.

Figure 1. a: Moderately enhancing lesion profile, *C(t)*, generated using simulation parameters $K^{trans} = 0.4$ minute^{-1}, $v_e = 0.3$. *T* is the overall scan duration. **b:** K-space power spectrum $C(k_t)$, whose maximum extent is defined as $\pm K_t/2$.

Let *T* be the total duration of the DCE experiment, within which most of the dynamic change of interest occurs. The total number of sample points that can be acquired, *N*, is given by:

$$N = T/\Delta t. \quad (2)$$

The maximum allowable spatial bandwidth *Ky* is then given as

$$Ky = N/FOVy \quad (3)$$

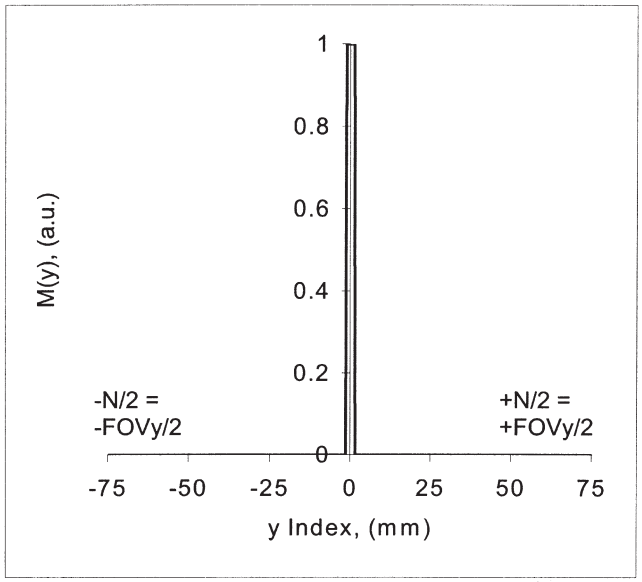

a.

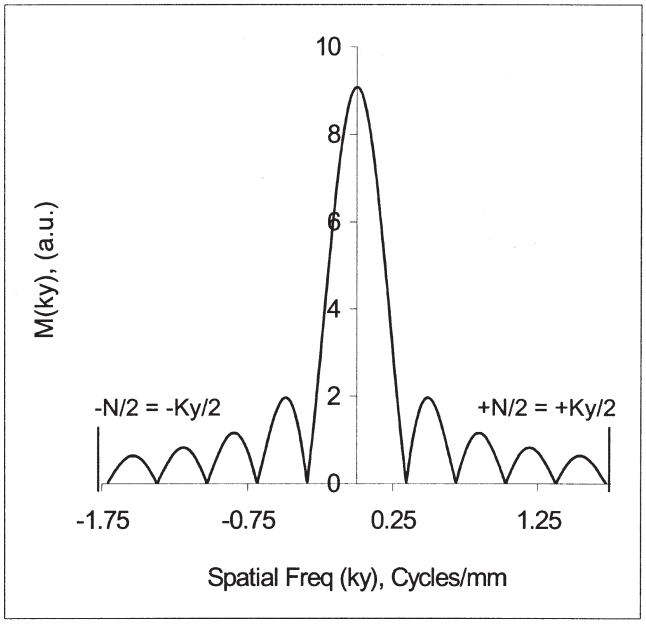

b.

Figure 2. a: Spatial profile, *M(y)*, of an object 12 pixels wide along the y-axis. **b:** K-space power spectrum, $M(k_t)$.

For example, choosing nominal values of $Nz = 32$, TR = 10 msec, and $T \sim 4$ minutes, N = the 640 total measurements that can be made at sampling intervals $\Delta t = 0.32$ seconds. For these imaging parameters, consider a small lesion, *M(y)*, approximately 2% of the nominal field of view (FOV) (12 pixels in a 640 matrix), with the spatial profile shown in Fig. 2a. The corresponding k-space spectrum, $M(k_y)$, obtained by taking the Fourier transform of the 1D object function, is limited in extent from $-Ky/2$ to $Ky/2$ (Fig. 2b).

Analogous to the spatial arguments, the maximal temporal bandwidth is also defined by the rate of digitization and is given as

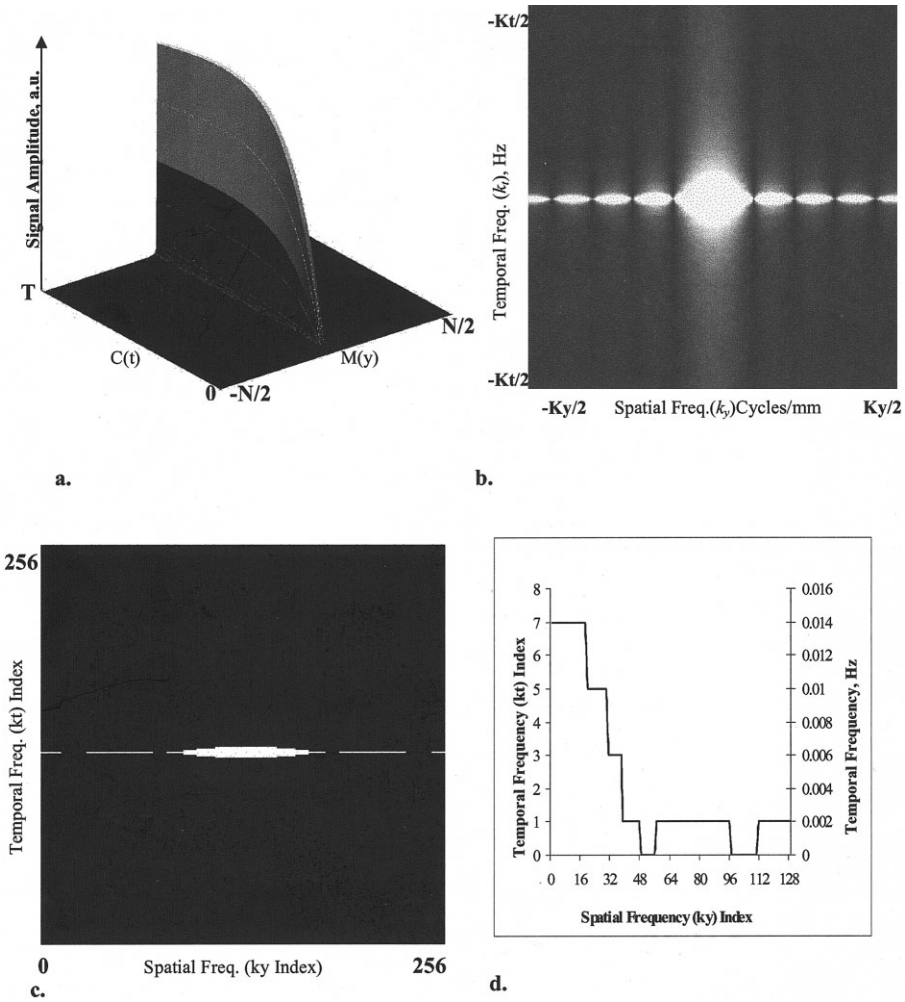

Figure 3. **a:** Combined 2D spatio-temporal object. **b:** k_y-k_t representation of spectral power in dual object. **c:** Thresholded region encompassing N sample points containing maximal spectral energy in k_y-k_t. **d:** Spatial and temporal sampling bandwidth pairs.

$$K_t = 1/\Delta t = N/T \quad (4)$$

For the lesion enhancement profile shown in Fig. 1a, the corresponding spectral profile is its Fourier transform, $C(k_t)$, limited in extent to $\pm K_t/2$, as shown in Fig. 1b. The maximal spectral bandwidths, in effect, describe the theoretical limits on the sampling rate for each of the spatial and temporal functions individually.

Spatio-Temporal k_y-k_t Space Representation

We begin by modeling the spatial and temporal functions up to N-point resolution; i.e., it is assumed that each function is sampled at the theoretical maximal rate permitted by the imaging constraints. The instantaneous signal from a lesion is the product of the spatial amplitude $M(y)$ and the modulating contrast $C(t)$. However, the spatial features are completely unrelated to the temporal characteristics; i.e., $M(y)$ and $C(t)$ are completely distinct functions ($M(y,t) = M(y) \cdot C(t)$). Thus, it is possible to construct a combined 2D spatio-temporal object wherein the object spatial profile is represented along one axis, and the temporal change, that amplitude modulates the spatial profile, is represented along an orthogonal dimension (Fig. 3a). Fourier transformation of the 2D ($N \times N$) space-time object yields the k_y-k_t spectral map (Fig. 3b). This is mathematically the outer product of the Fourier spectra of the object spatial and enhancement profiles, $\hat{M}(ky)^T \cdot \hat{C}(kt)$. The k_y-k_t map, in effect, encompasses the spectral space that would be sampled if both spatial and temporal functions were simultaneously sampled at the maximum allowable bandwidths; i.e, N^2 samples were acquired. This establishes the spectral space that can potentially be sampled during the imaging experiment. In practice, it is not possible to sample this entire space, since we are constrained by the imaging experiment to a maximum of N samples. However, all possible schemes of temporal and spatial sampling are included within the k_y-k_t map. For example, in the limit, we could sample the spatial function up to N-point resolution and acquire a single temporal sample or vice versa.

Segmentation of k_y-k_t Plane

The k_y-k_t spectral map is a representation of the combined spectra of N temporal and N spatial samples. However, for the given imaging constraints, it is possible to obtain a *total* of only N measurements within the k_y-k_t space. The objective is to choose the subset of N points from within the k_y-k_t space, independent of bias toward either the spatial or temporal function. The following energy maximization criterion is chosen as the basis for sampling the k_y-k_t map:

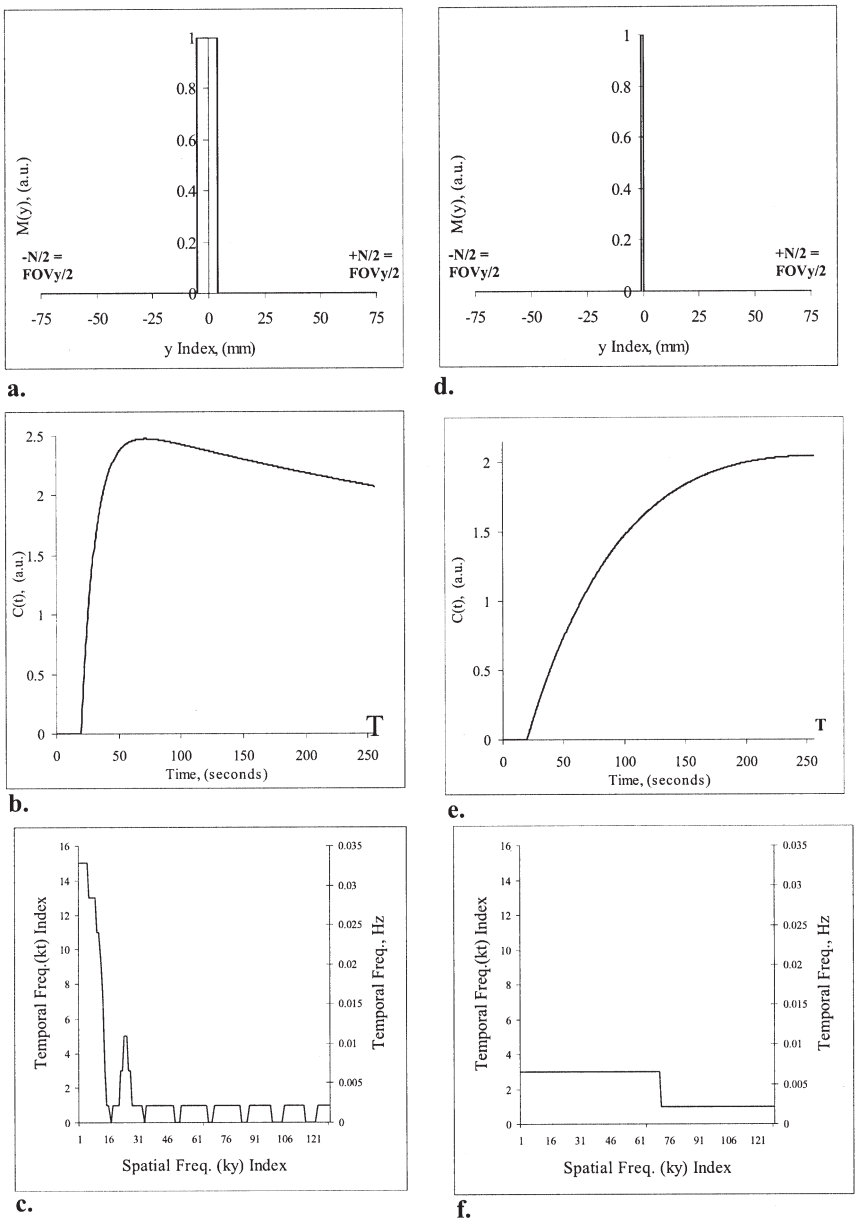

Figure 4. a: Large (30-pixel) object exhibiting. **b:** Rapid enhancement (K^{trans} = 1.5 minute^{-1}, v_e = 0.3. **c:** Associated spatio-temporal sampling prescription. **d** and **e:** Similar analysis for very small object (three pixels) with slow enhancement (K^{trans} = 0.2 minute^{-1}, v_e = 0.3). For the large, rapidly enhancing object, it is recommended that the central (16 k_y) lines be imaged at a higher temporal rate, up to 16 samples. Conversely, for the small, slowly enhancing object, the central (68 k_y) lines should be sampled at a slower temporal rate, three samples.

$$\text{MAX} \sum_{(ky,kt)\in S} |\hat{M}(ky)|^2 |\hat{M}(kt)|^2$$

$$\text{such that } |S| \le N, \text{ and } S \in K$$

$$K = \{(k_y, k_t): 1 \le k_y \le N, 1 \le k_t \le N\} \qquad (4)$$

where $|\hat{M}(k_y)^2| \cdot |\hat{C}(kt)|^2$ is the instantaneous spectral power in the enhancement-modulated object and N is the total number of samples that can be acquired. This yields an area plot within the k_y-k_t domain that contains the greatest total spectral power for the given spatio-temporal object, constrained by N samples. For any given spatial bandwidth included in this area, the corresponding maximum temporal bandwidth prescription is automatically selected; i.e., we can determine k_y-k_t bandwidth pairs. For the enhancing object in Fig. 3a, a binary thresholded map representing the optimal energy sampling region is shown in Fig. 3c. It is convenient to look at a binary thresholded map because this directly yields the sampling prescription, since each bandwidth corresponds to a specific number of measurements or index point along the k_t or k_y axis (Fig. 3d). Thus for the given spatio-temporal object, the sampling prescription can be summarized in a plot of the temporal samples/bandwidth per spatial index/bandwidth (see Fig. 3d). For the simulated spatio-temporal object (Fig. 3a), the recommended variable-rate acquisition is as follows: the central 36 k_y lines should be sampled at least seven times (252 samples), the next 11 lines on each side of the symmetric k_y axis at least five times (55 samples), and so on, proceeding until the total number of sample points N = 640. Typically, the sampling rate for the central k_y lines is highest and determines the overall temporal sampling rate. This result is consistent with the notion that the bulk of the

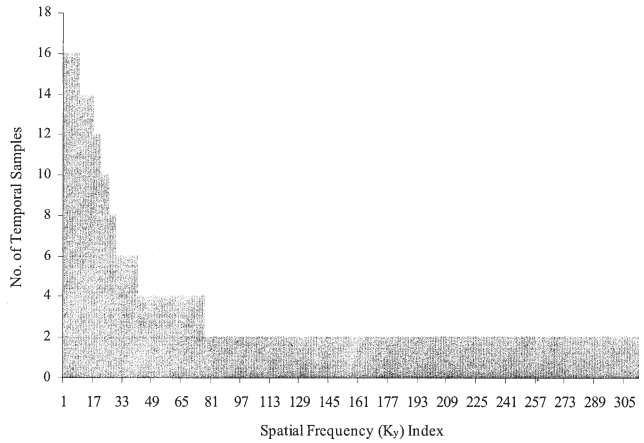

Figure 5. Number of temporal samples prescribed by STBB analysis over all simulated spatio-temporal objects, per spatial frequency index. The global maximum number of temporal samples for segments in k_y of width four lines was used.

dynamic change information is encoded in the lower spatial frequencies. For peripheral segments that are sampled at a slower rate, missing data can be generated by linear interpolation between acquired segments. Figure 4 shows two additional examples of enhancing lesions. The k_y -k_t analysis suggests that fewer central k-space lines should be imaged at a higher temporal rate for a rapidly enhancing large object. Conversely, for the slowly enhancing small object, larger central spatial bandwidth should be acquired at a relatively slower temporal rate.

Implementation of STBB Analysis

So far the k_y-k_t representation and the associated sampling prescriptions have been considered for individual enhancing objects. This method is applicable when one can define a single targeted object. That is, we can anticipate the signal enhancement as well as the spatial features that must be characterized. However, in practice, one may wish to image a range of spatio-temporal objects. Ideally, the variable-rate acquisition should be designed such that it is applicable to a continuum of object spatial features and enhancement characteristics. In order to do this, we begin by conducting the STBB analysis for a finite set of spatio-temporal objects. Subsequently, we develop an acquisition scheme that is optimized over all these objects.

Variable-Rate Acquisition Scheme

For breast lesions we consider three broad classes of lesion spatial and temporal properties as a representative subset. Lesions are modeled as small, medium, and large, permuted with slow, moderate, and rapid enhancement conditions. For purposes of simulation, three spatial object functions (2, 10, and 30 pixels wide) and three enhancement functions (K^{trans} = 1.5, 0.4, and 0.2 minute^{-1}, v_e = 0.3) were chosen. All simulations were done using Matlab (Natick, MA). Using the STBB analysis discussed earlier, spatio-temporal bandwidth pairs were obtained for each individual enhancing object. The next step is to reduce the several individual prescriptions to a single value optimal for all cases. This was done by selecting a maximum temporal sampling rate, over all spatio-temporal objects, for any given spatial bandwidth as the prescription. As a simplification for ease of implementation, the global maximum number of temporal samples for segments in k_y of width four lines was chosen as the prescription. Figure 5 shows the variable-rate sampling prescription for the ensemble of simulated conditions. The resulting recommended coverage is as follows: The central eight k_y lines should be sampled 16 times over the modeled four-minute enhancement period. The next eight lines on each side of the symmetric k_y-axis should be sampled 14 times, and so on. Beyond a spatial bandwidth of 72 lines, two temporal samples should be acquired. Thus, for the class of spatio-temporal objects under consideration, the guidelines for choosing the temporal sampling rate for any given spatial frequency segment have been established.

The next stage is to design a practical variable-rate acquisition scheme. The STBB analysis does not preclude use of partial-Fourier acquisition (32); therefore, this method was incorporated to effectively increase k_y coverage without increasing scan duration. One such partial-Fourier acquisition that implements the sampling prescriptions recommended by the STBB analysis (Fig. 5) is shown in Fig. 6. The resulting scheme had a nominal reconstructed matrix size in k_y = 144 with 40 k_y lines acquired per time point, including eight additional lines over half matrix. One pre- and one postdy-

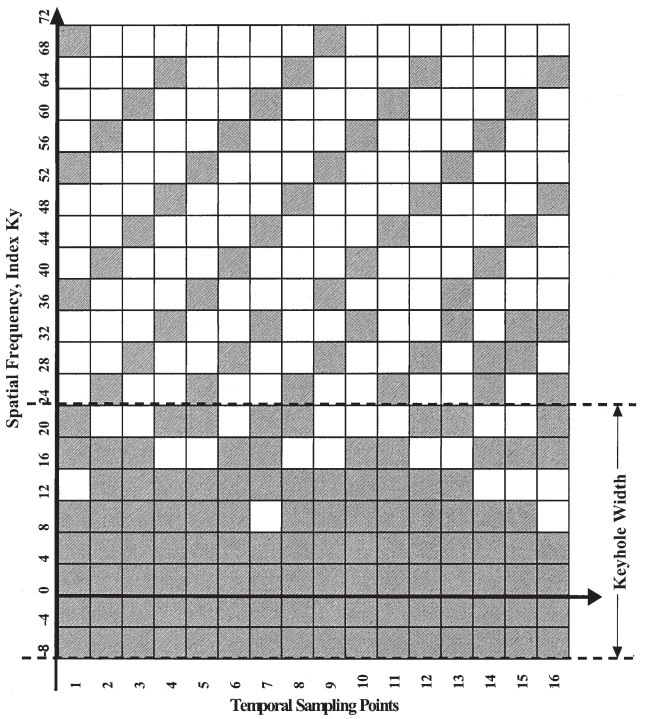

Figure 6. Partial k-space variable-rate acquisition, using prescriptions shown in Fig. 5. The central 16 k_y lines are sampled 16 times, the next 4 k_y lines are sampled 14 times, and so on. The corresponding keyhole acquisition with 40 central k_y lines sampled 16 times is also shown.

Table 1
Summary of Estimated K^{trans} and v_e

No.	Simulation parameters Ve = 0.3	K^{trans}, min^{-1}		v_e	
		Keyhole	STBB	Keyhole	STBB
1	K^{trans} = 1.5 min^{-1} Npix = 2	0.78	1.1	0.12	0.28
2	K^{trans} = 1.0 min^{-1} Npix = 5	0.74	0.53	0.25	0.26
3	K^{trans} = 0.6 min^{-1} Npix = 10	0.52	0.53	0.26	0.27
4	K^{trans} = 0.4 min^{-1} Npix = 15	0.34	0.35	0.25	0.27
5	K^{trans} = 0.3 min^{-1} Npix = 20	0.29	0.28	0.27	0.25
6	K^{trans} = 0.2 min^{-1} Npix = 30	0.19	0.18	0.28	0.28

namic acquisition with matrix size in k_y = 144 were also included in the acquisition.

Computer Simulations

The particular STBB scheme (Fig. 6) was evaluated by applying it to a range of spatio-temporal objects. We chose object sizes Npix = 2, 5, 10, 15, 20, and 30 pixels and permuted these with enhancement rates K^{trans} = 1.5, 1, 0.6, 0.4, 0.3, and 0.2 $minute^{-1}$. The extracellular volume fraction v_e was held at 0.3. Partial-Fourier keyhole acquisition with repeated sampling of the same 40 k_y lines per time point is shown in Fig. 6. Reconstruction of keyhole data was done by substituting peripheral k-space lines from an initial full matrix data set. Data from STBB simulations were reconstructed by linearly interpolating between acquired k_y lines to generate missing data. Mean region-of-interest (ROI) calculations were performed using the original simulated object as a mask, to generate mean enhancement profiles. The enhancement curves were fitted to the model used in simulation to calculate K^{trans} and v_e.

The STBB scheme (Fig. 6) was tested for an additional spatio-temporal object modeled as a 1D rim-enhancing lesion. The tumor was modeled as 10 pixels wide with a 3-pixel rim. The simulated enhancement parameters were K^{trans} = 2 $minute^{-1}$ in rim and 1 $minute^{-1}$ within, v_e = 0.3.

RESULTS

The estimated values for K^{trans} and v_e are summarized in Table 1. The STBB scheme results in more accurate estimation of the rate and extracellular volume fraction parameters when the object size is small (two and five pixels) and the enhancement rates are rapid (1.5 and 1 $minute^{-1}$), compared to the keyhole acquisition. As the object size increases or, conversely, the enhancement rates decrease, both schemes perform comparably well. The comparison of the STBB scheme with keyhole acquisition in terms of eliciting the spatial function is shown in Fig. 7. The reconstructions are shown for the time point at which peak enhancement is reached. For a rapidly enhancing small object (Npix = 2, K^{trans} = 1.5 $minute^{-1}$), shown in Fig. 7a, there is noticeable broadening of line width with the keyhole reconstruction, while the STBB reconstruction closely approximates the original simulated object. Figure 7b shows the comparison for a large, slowly enhancing object (Npix = 30, K^{trans} = 0.2 $minute^{-1}$). In this case, the reconstructed object is similar for both schemes and very close to the original simulated object. In general, the STBB scheme provides higher spatial fidelity for very small objects. As the object size increases, all schemes performed comparably.

The results in Table 2 show that, again, the STBB scheme estimates the enhancement parameters more accurately. In Fig. 8, which shows the spatial profiles at peak enhancement, the keyhole reconstruction shows higher spatial blur than the STBB reconstruction.

CONCLUSIONS

In this paper, a method to design a variable-rate acquisition scheme has been developed and illustrated for breast imaging. One particular scheme (Fig. 6) devised using the STBB analysis was applied to a sample set of simulated lesions. The scheme was found to perform as well or better than standard and partial-Fourier keyhole imaging in terms of enhancement parameter estimation and characterization of spatial detail. The STBB analysis has the potential to be extended to any dynamic imaging condition. The set of a priori objects included in modeling can be modified—for example, if one is interested only in characterizing rapidly enhancing breast tumors, the K^{trans} values used in modeling can range from (0.6–2 $minute^{-1}$) and a corresponding acquisition scheme can be derived. Similarly, lesions ranging in size less of than 1 cm alone could be included in modeling if characterization of very small lesions alone is desired.

Closer inspection of the STBB analysis shown in Figs. 3 and 4 indicates that higher temporal sampling rates are prescribed for rapidly enhancing objects and larger extents of coverage along k_y are recommended for small objects. This is fairly intuitive since it is expected that rapid dynamic change will possess higher energies over a larger bandwidth, as will a small spatial object. It also underscores the point that the STBB formalism is an

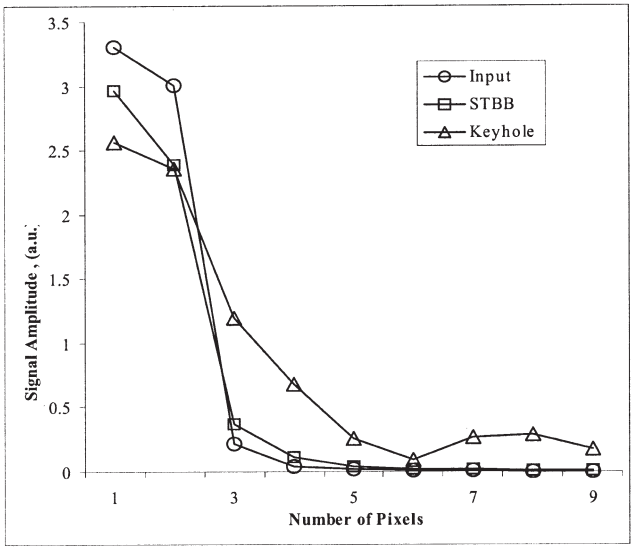

a.

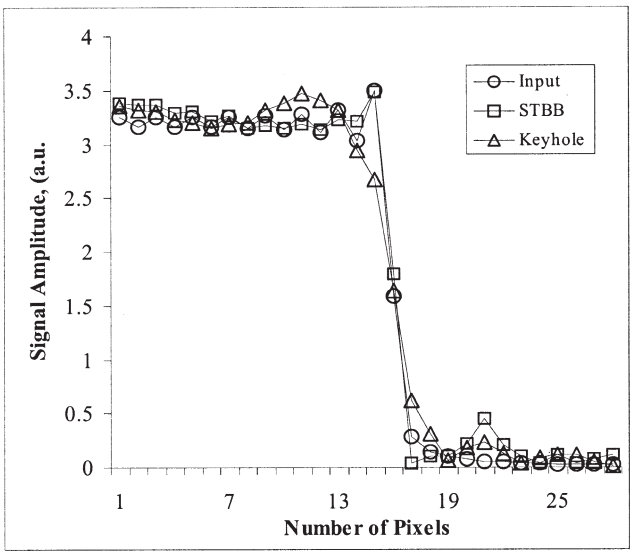

b.

Figure 7. **a:** Comparison of STBB and keyhole acquisitions. Rapid enhancement (K^{trans} = 1.5 minute^{-1} and v_e = 0.3) and small (two-pixel) object. The keyhole reconstruction shows higher spatial blur. **b:** Slow enhancement (K^{trans} = 0.2 minute^{-1} and v_e = 0.3) and large (30-pixel) object.. For purposes of clarity, the region where the bulk of the simulated object is contained has been shown. There was negligible reconstruction artifact in the peripheral FOV.

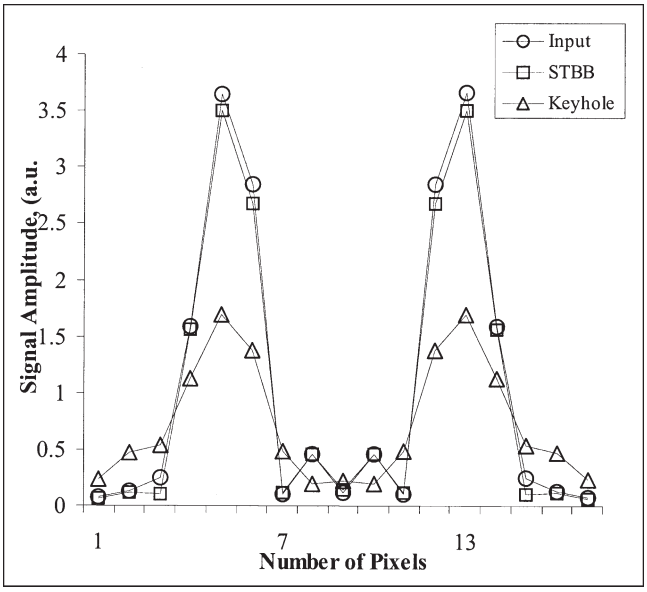

Figure 8. Comparison of STBB and keyhole acquisitions for rim-enhancing object (K^{trans} = 2 minute^{-1} and v_e = 0.3), 10-pixel object with 3-pixel rim. The keyhole reconstruction shows higher spatial blur.

objective mechanism to balance spatial and temporal samples rather than a numerical optimization scheme based on a specific pharmacokinetic model and given object. Neither the temporal nor the spatial properties alone determine the resulting coverage prescriptions. Since the spectral samples in k_y-k_t space are weighted by both the spatial and temporal spectral densities, it is the net energy contribution of a given k_y-k_t sample that serves as the inclusion criterion. Thus, while the STBB method permits user input in selecting the class of spatio-temporal objects that might be encountered in the DCE-MRI experiment, the resulting acquisition scheme is optimized over all anticipated objects.

In this paper, we reduce 3D imaging to a single spatial axis under the assumption that when imaging at a TR of ~10 msec and for our chosen nominal spatial resolution, the x- and z-encodings occur relatively faster than the contrast enhancement changes. This assumption may not hold when quantifying very rapidly varying functions such as the arterial input function, where the entire dynamic change could occur within the duration of a single volume acquisition. For such a case, the STBB approach may not prove to be advantageous in designing an image acquisition scheme, unless it is possible to further reduce the TR or consider segmentation along an addition spatial axis.

Table 2
Estimated Ktrans and v_e for Rim Enhancing Object

No.	Simulation parameters Ve = 0.3	K^{trans}, min^{-1}		v_e	
		Keyhole	STBB	Keyhole	STBB
1	K^{trans} = 2.0 min^{-1} Rimpix = 2	1.1	1.53	0.22	0.24
2	K^{trans} = 1.0 min^{-1} Npix = 7	0.79	0.81	0.24	0.27

In conclusion, we have demonstrated an intuitive formalism applicable to DCE-MRI for a set of targeted dynamic events as well as spatial features. This formalism was developed for a set of object and enhancement characteristics typically observed in DCE-MRI of breast tumors to yield a suitable variable-rate acquisition scheme.

ACKNOWLEDGMENTS

We thank Dr. Jeffrey Fessler and Dr. Robert Welsh for their valuable suggestions and assistance in reviewing this manuscript.

REFERENCES

1. Turner R. Signal sources in bold contrast fMRI. Adv Exp Med Biol 1999;413:19–25.
2. Howseman AM, Bowtell RW. Functional magnetic resonance imaging: imaging techniques and contrast mechanisms. Philos Trans R Soc Lond B Biol Sci 1999;354:1179–1194.
3. Pettigrew RI. Dynamic cardiac MR imaging. Techniques and applications. Radiol Clin North Am 1989;27:1183–1203.
4. Barger AV, Grist TM, Block WF, Mistretta CA. Single breath-hold 3D contrast-enhanced method for assessment of cardiac function. Magn Reson Med 2000;44:821–824.
5. White RD, Paschal CB, Tkach JA, Carvlin MJ. Functional cardiovascular evaluation by magnetic resonance imaging. Top Magn Reson Imaging 1990;2:31–48.
6. Schoenberg SO, Bock M, Knopp MV, et al. Renal arteries: optimization of three-dimensional gadolinium-enhanced MR angiography with bolus-timing-independent fast multiphase acquisition in a single breath hold [Comments]. Radiology 1999;211:667–679.
7. Lorenz CH, Johansson LO. Contrast-enhanced coronary MRA. J Magn Reson Imaging 1999;10:703–708.
8. Taylor JS, Tofts PS, Port R, et al. MR imaging of tumor microcirculation: promise for the new millennium. J Magn Reson Imaging 1999;10:903–907.
9. Kim YR, Savellano MD, Weissleder R, Bogdanov Jr A. Steady-state and dynamic contrast MR imaging of human prostate cancer xenograft tumors: a comparative study. Technol Cancer Res Treat 2000; 6:489–495.
10. Thomas AL, Morgan B, Drevs J, et al. Vascular endothelial growth factor receptor tyrosine kinase inhibitors: PTK787/ZK 222584. Semin Oncol 2003;30:32–38.
11. Lee SV, Lavelle MT, Rofsky NM, et al. Hepatic MR imaging with a dynamic contrast-enhanced isotropic volumetric interpolated breath-hold examination: feasibility, reproducibility, and technical quality. Radiology 2000;215:365–372.
12. Nunes LW, Schnall MD, Siegelman E, et al. Diagnostic performance characteristics of architectural features revealed by high spatial-resolution MR imaging of the breast. AJR Am J Roentgenol 1997; 169:409–415.
13. Tofts PS, Berkowitz B, Schnall MD. Quantitative analysis of dynamic Gd-DTPA enhancement in breast tumors using a permeability model. Magn Reson Med 1995;33:564–568.
14. Hoffmann U, Brix G, Knopp MV, et al. Pharmacokinetic mapping of the breast: a new method for dynamic MR mammography. Magn Reson Med 1995;33:506–514.
15. Flickinger FW, Allison JD, Sherry FM, Wright JC. Differentiation of benign from malignant breast masses by time-intensity evaluation of contrast enhanced MRI. Magn Reson Imaging 1993;11:617–620.
16. Stack JP, Redmond OM, Codd MB, et al. Breast disease tissue characterization with Gd-DTPA enhancement profiles. Radiology 1990;174:491–494.
17. Evelhoch JL. Key factors in the acquisition of contrast kinetic data for oncology. J Magn Reson Imaging 1999;10:254–259.
18. Tuncbilek N, Unlu E, Karakas HM, Cakir B, Ozyilmaz F. Evaluation of tumor angiogenesis with contrast-enhanced dynamic magnetic resonance mammography. Breast J 2003;9:403–408.
19. Xiang QS, Henkelman RM. K-space description of MR imaging of dynamic objects. Magn Reson Med 1993;29:422–428.
20. Spielman DM, Pauly JM, Meyer GH. Magnetic resonance fluoroscopy using spirals with variable sampling densities. Magn Reson Med 1995;34:388–394.
21. Doyle M, Walsh EG, Blackwell GG, Pohost GM. Block regional interpolation scheme for k-space (BRISK): a rapid cardiac imaging technique. Magn Reson Med 1995;33:163–170.
22. Liang ZP, Jiang H, Hess CP, Lauterbur PC. Dynamic imaging by model estimation. Int J Imag Syst Technol 1997;8:551–557.
23. Daniel BL, Yen YF, Glover GH, et al. Breast disease: dynamic spiral MR imaging [Comments]. Radiology 1998;209:499–509.
24. Hulka CA, Edmister WB, Smith BL, et al. Dynamic echo-planar imaging of the breast: experience in diagnosing breast carcinoma and correlation with tumor angiogenesis. Radiology 1997;205:837–842.
25. Chenevert TL, Helvie MH, Aisen AM, et al. Dynamic three-dimensional imaging with partial k-space sampling: initial application for gadolinium-enhanced rate characterization of breast lesions. Radiology 1995;196:135–142.
26. Parrish T, Hu X. Continuous update with random encoding (CURE): a new strategy for dynamic imaging. Magn Reson Med 1995;33:326–336.
27. Madore B, Glover GH, Pelc NJ. Unaliasing by Fourier-encoding the overlaps using the temporal dimension, applied to cardiac imaging and fMRI. Magn Reson Med 1999;42:813–828.
28. Wu Y, Alexander AL. Temporal frequency analysis of dynamic MRI techniques. Magn Reson Med 2001;45:550–556.
29. Schnall MD, Ikeda DM. Technical report of the international working group on breast MRI. Lesion Diagnosis Working Group report. J Magn Reson Imaging 1999;10:982–990.
30. Tofts PS, Kermode AG. Measurement of the blood-brain barrier permeability and leakage space using dynamic MR imaging. 1. Fundamental concepts. Magn Reson Med 1991;17:357–367.
31. Tofts PS, Brix G, Buckley D, Evelhoch JL, et al. Estimating kinetic parameters from dynamic contrast-enhanced T1-weighted MRI of a diffusable tracer: standardized quantities and symbols. J Magn Reson Imaging 1999;10:223–232.
32. McGibney G, Smith MR, Nichols ST, Crawley A. Quantitative evaluation of several partial Fourier reconstruction algorithms used in MRI. Magn Reson Med 1993;30:51–59.